Flow Light Scattering Studies of Polymer Coil Conformation in Solutions in Extensional Flow

Ellen C. Lee and Susan J. Muller*

Department of Chemical Engineering, University of California, Berkeley, and Center for Advanced Materials, Lawrence Berkeley National Laboratory, Berkeley, California 94720

Received August 11, 1998; Revised Manuscript Received March 2, 1999

ABSTRACT: The dynamics of isolated polymer chains in dilute solution under steady, extensional flow were investigated by means of flow light scattering. Both the orientation and deformation of the chains during flow were determined by analyzing the angular dependence of the scattered light intensity. The extensional flow field was imparted on the polymeric fluids by a stagnation point flow in the center of a four-roll mill apparatus. The fluids studied were nearly monodisperse high molecular weight polystyrenes (HMPS) of various molecular weights dissolved in either the viscous solvent dioctyl phthalate (DOP) or a mixed solvent of low molecular weight polystyrene (LMPS) and dioctyl phthalate. The flow field in a Newtonian fluid of seeded glycerin was also examined by flow dynamic light scattering techniques and flow visualization to confirm the extensional flow field. Flow dynamic light scattering and flow visualization results verified that the field generated by the four-roll mill was a reasonable approximation of planar extensional flow, under the conditions investigated. Flow (static) light scattering results confirmed that the polymer chains aligned completely with the stretch direction, as expected for this type of flow. The deformation of the chains, however, was significantly less than predicted by elastic dumbbell models. Also studied were the effects of molecular weight and solvent quality on the deformation of the polymer chains. Comparisons are drawn between polystyrene chains in the strong extensional flow field studied here and a steady shearing flow examined in a previous publication as well as with other studies in extensional flows.

Introduction

The extensional behavior of polymeric liquids gives them unique and desirable characteristics for many applications. The manufacture of fibers is made possible due to the extensibility of the polymer chains, and the elongation of single chains in very dilute solutions is thought to play a key role in the phenomenon of drag reduction in turbulent flow.[2,3] The striking increase in elongational viscosity over the shear viscosity also suggests that the dynamics of the polymer molecules in extension differ dramatically from those in shear. As a result, there has been much interest in studying chain dynamics in extensional flows.

One common technique of imposing an extensional flow field on a fluid sample is by use of stagnation point flow. Stagnation point flows are used to increase the residence time of a polymer within the strong velocity gradient. Two methods have been typically used to impart a stagnation point flow: the flow of fluid into two opposed jets or opposed slots, pioneered by Keller and Odell and co-workers,[4−7] and the flow in the center of four rollers of a four-roll mill device, first proposed by Taylor[8] and extensively studied by Leal et al.[9−14] In the opposed jets flow, two nozzles are directed toward one another. The fluid enters the nozzles to produce extension in the direction parallel to the axis connecting the nozzles. This geometry creates a uniaxial extensional flow. The opposed slots flow is similar, but instead of nozzles, the fluid flows into opposed slots to produce a planar extensional flow. In the four-roll mill, the rollers are rotated in the manner shown in Figure 3b, such that it also produces a planar extensional flow. While stagnation point flows allow extension of some fluid elements to extremely high strains, the strain history of all fluid elements is not homogeneous, and fluid on streamlines far from the stagnation streamline undergo little strain. Contraction flows have also been used to generate transient elongational flows.[2,15] Here, the flow in the central core is primarily extensional, but due to the absence of a stagnation point, fluid elements necessarily experience a limited amount of strain.

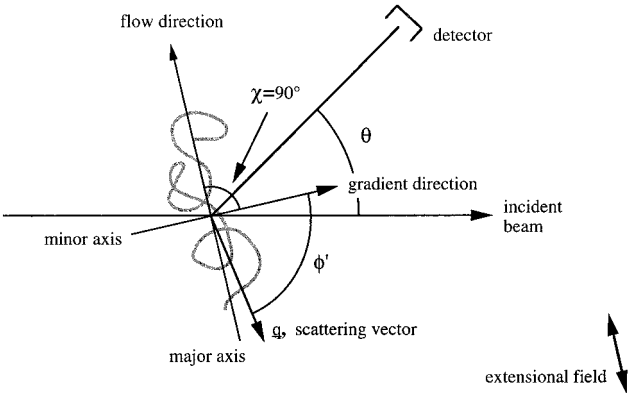

Figure 1. Shape of a deformed polymer coil in extensional flow, showing the major and minor axes, as well as the flow direction. The orientation angle, χ, and the flow plane angle, ϕ', are shown for specific (arbitrary) detector angle, θ.

Rheological measurements in extensional flows of polymer solutions typically show Trouton ratios (i.e., the ratio of extensional to shear viscosity) that exceed the value of three seen for Newtonian fluids by several orders of magnitude. The extensional viscosity reaches an asymptote at high dimensionless strains $\dot{\epsilon}\lambda$, where $\dot{\epsilon}$ is the extension rate and λ is the characteristic relaxation time of the polymer, suggesting complete extension of the polymer molecules.[16] However, calculations of both the strain needed to reach full extension and the magnitude of the extensional viscosity corresponding

10.1021/ma981277a CCC: $18.00
Published on Web 04/22/1999

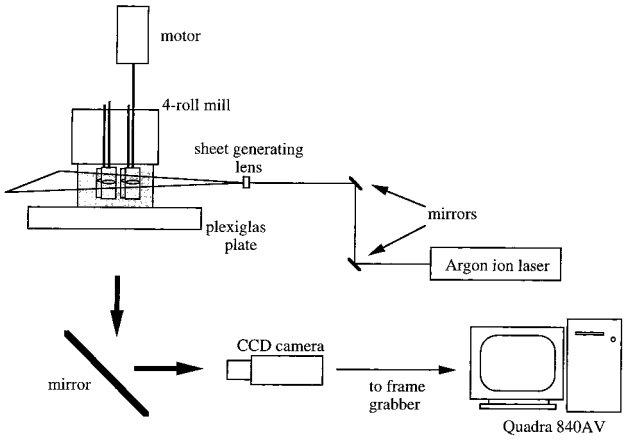

Figure 2. Schematic of flow visualization setup for extensional flow.

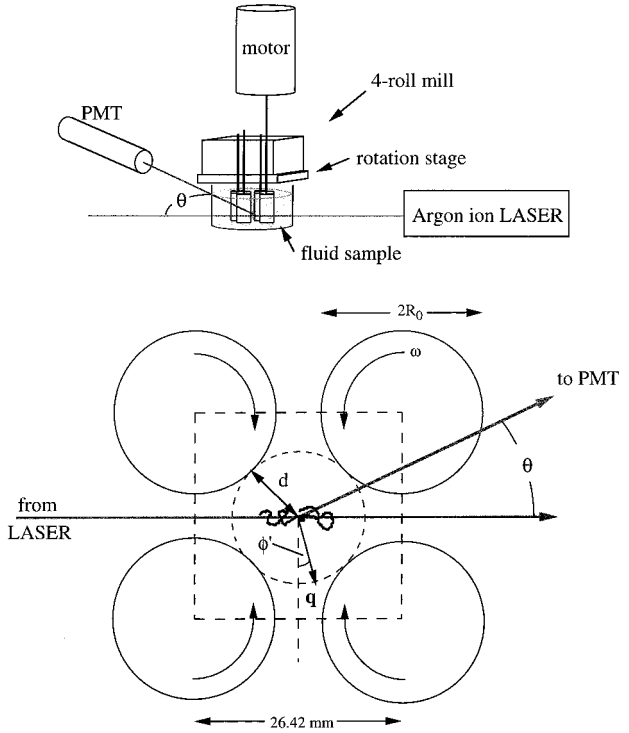

Figure 3. Flow light scattering apparatus: (a, top) side view of four-roll mill light scattering apparatus; (b, bottom) top view of four-roll mill geometry. The radius of the rollers is $R_0 = 10$ mm; the radius of the circle whose circumference just touches the rollers is $d = 8.68$ mm. ω is the angular velocity.

to fully stretched chains indicate that the molecules never reach full extension.[17]

Birefringence measurements in extensional flow from a number of groups also suggest the polymer undergoes a coil−stretch transition from a coil to a fully extended state at a dimensionless strain rate $\dot{\epsilon}\lambda$ of order one. Keller and co-workers, Fuller and co-workers, and Menasveta and Hoagland all report a rapid increase of the measured birefringence as the strain rate is increased through a critical value $\dot{\epsilon}_c$, followed by a saturation of the birefringence at still higher strain rates.[5,7,11,18] In a comprehensive series of studies, Keller, Odell, and co-workers at Bristol have demonstrated that the critical strain rate $\dot{\epsilon}_c$ corresponds to $1/\lambda_z$, where λ_z is the Zimm relaxation time, and that the dependence of $\dot{\epsilon}_c$ on molecular weight is consistent with the Zimm model. In addition, they were able to demonstrate chain halving at high strain rates and a dependence of the strain rate for fracture on molecular weight that is consistent with fully extended chains.[4−7,19−21] The level of saturation birefringence is also roughly consistent with full extension of the chains, although as Carrington et al. recently discuss, birefringence is a measure of the local segmental orientation, rather than a direct measure of global chain conformation, and prediction of birefringence values for a fully extended molecule in solution is complex. Carrington et al. also demonstrate that the magnitude of the maximum measured birefringence is an increasing function of molecular weight. They interpret this as meaning the polymers are not fully extended: in lower molecular weight chains an increased proportion of the chain ends are involved in relatively unstretched coillike structures. These authors also illustrate the extreme localization of the region of stretching (in the opposed jets flow, the region was observed to be on the order of 30 μm in diameter) as well as significant flow modification by the chain stretching which persists to remarkably low concentrations (an order of magnitude or more below c^*).[22,23]

In the four-roll mill, the localization of chain stretching and the effects of concentration on the flow field have been studied by Leal and co-workers using birefringence and a homodyne light scattering technique (referred to as flow dynamic light scattering below).[11,24,25] Dunlap and Leal performed birefringence measurements in both the simple shear flow in a two-roll mill and the two-dimensional extensional flow in a four-roll mill for dilute solutions of polystyrene. For a single molecular weight polystyrene in different solvents, the onset of birefringence scaled with the Zimm relaxation time; but the maximum or saturation value of birefringence depended on solvent, and the highest value was found in the two-roll mill rather than the four-roll mill. Their velocity gradient measurements indicate once the polymers become sufficiently extended (but before the birefringence saturates), there is a measurable decrease in the velocity gradients which becomes larger away from the stagnation point and extends well beyond the region of high polymer extension and high flow birefringence. The onset of flow modification appears to occur once the polymers are stretched such that their volume concentration (calculated using a sphere diameter equal to the extended length) is approximately 5000.[25]

Two methods have been used to measure directly the stretching of polymer chains in extensional flow. For synthetic polymers including poly(ethylene oxide), polyisobutylene, and polystyrene, light scattering techniques have been used to obtain average measurements of chain conformation during extensional flow. In quiescent solutions, total intensity light scattering has long been used to characterize the size, molecular weight, and solvent quality of polymers in dilute solution by examining the angular dependence of the scattered light. The radius of gyration $\langle r_g^2 \rangle^{1/2}$ can be determined from the angular dependence of the scattered light intensity independent of the shape of the scatterer provided the measurements can be made at sufficiently low scattering angles. The technique can also be applied to flowing solutions, as first suggested by Peterlin in 1957,[26] and a number of studies of synthetic polymer orientation and deformation in shear flow have been published.[1,27−29] In all of these flow light scattering studies, the amount of deformation measured in shear-

ing flow was much lower than predicted by bead−spring kinetic theories.

Only three previous investigations have used flow light scattering to examine polymer chain dynamics in extensional flows. In 1977, Lumley[2] used light scattering to study the transient extensional flow of a dilute poly(ethylene oxide) solution through a two-dimensional contraction and reported expansions of a factor of 4; i.e., the radius of gyration projected onto the stretching axis reached 4 times the equilibrium radius of gyration. Smith et al.[15] studied dilute solutions of polyisobutylene in an axisymmetric contraction flow and found similar results: the extension ratios achieved were no more than four. In addition, in comparing polyisobutylenes of two molecular weights, these authors found that scaling the data with the relaxation time did not collapse the two data sets, and the lower molecular weight polymer stretched more than the higher molecular weight polymer at comparable Deborah number. More recently, Menasveta and Hoagland[30] studied a solution of a single ultrahigh molecular weight (2.0×10^7 g/mol) polystyrene sample dissolved in toluene in flow through opposed jets. Here they found that at the stagnation point the maximum extension ratio $\langle r_g^2\rangle_{\dot\epsilon\lambda}^{1/2}/\langle r_g^2\rangle_0^{1/2}$ was roughly 2, even at a dimensionless strain rate of $\dot\epsilon\lambda \approx 20$.

The second method that has been used to measure directly the stretching of polymer chains in extensional flow is fluorescence microscopy. While most synthetic polymers are too small to be observed directly through this technique, Chu and co-workers have investigated the dynamics of DNA molecules by direct visualization of fluorescently labeled chains.[31−34] In a planar elongational flow generated by a cross-slot geometry, Perkins et al.[31] measured the extension as a function of strain for nearly 1000 separate λ bacteriophage DNA molecules and reported tremendous heterogeneity in the dynamics of the molecules: some appear to reach full extension, while others remain kinked, folded, or as nearly undeformed coils. The unfolding or stretching of a particular chain was sensitive to the molecule's initial conformation as it entered the region of high velocity gradient. At $\dot\epsilon\lambda \approx 3.3$, while some individual chains reached nearly full extension within 4 or 5 units of strain, the average extension was lower and did not reach steady state even by a strain of 5.7. Moreover, though, at $\dot\epsilon\lambda \approx 3.3$, the average chain extension even at fluid strains of 3 was nearly half the fully extended length of the molecule. For the DNA studied, which is about 400 persistence lengths, this corresponds to an extension ratio of $\langle r_g^2\rangle_{\dot\epsilon\lambda}^{1/2}/\langle r_g^2\rangle_0^{1/2}$ of about 5; however, comparable stretching of Menasveta and Hoagland's polystyrene, which consists of 8×10^4 persistence lengths, would result in $\langle r_g^2\rangle_{\dot\epsilon\lambda}^{1/2}/\langle r_g^2\rangle_0^{1/2}$ of roughly 30.

In this study, we use flow light scattering to measure the extension of high molecular weight polystyrene (HMPS) samples of varying molecular weight. A steady, extensional flow field was imposed by stagnation point flow in the center of a four-roll mill device. We confirm the flow field in the absence of polymer is a good approximation of extensional flow by flow visualization and flow dynamic light scattering techniques. Using the flow (static) light scattering technique, we study the conformation of the HMPS in solution during flow and examine the effects of polymer molecular weight and solvent quality on the deformation of the chains. Due to experimental limitations, we have achieved relatively modest dimensionless strain rates ($\dot\epsilon\lambda \approx 4$), so that, on the basis of a comparison to Dunlap and Leal or Carrington et al., we anticipate neither flow field modification due to the polymer nor full extension of the chains (i.e., we are at strain rates below those at which these authors observe saturation of the birefringence). In this limited strain rate regime, we examine the scaling of deformation by varying both molecular weight and monomer−solvent effects by using two different solvents at various temperatures. Also shown is a comparison of the extensional flow results to previous results[1] obtained in a steady shearing flow.

Theory

Light Scattering. Light scattering techniques are able to provide direct measurements of polymer chain shape and size, as well as molecular weight and solvent quality information. Because the size of the polymer molecules is on the order of the wavelength of the incident light, the light that is scattered from different points along a polymer chain undergoes destructive interference. The interference that occurs can be described by the molecule's form factor or particle scattering factor and depends on the size and shape of the molecule. By examining the angular dependence of the intensity of scattered light, size and shape information about the molecules in both quiescent and flowing solutions can be extracted. In the absence of information about the scatterer's shape, the radius of gyration can be determined in the limit $|\mathbf{q}|\langle r_g^2\rangle^{1/2} < 1$, where $|\mathbf{q}|$ is the magnitude of the scattering vector, $|\mathbf{q}| = (4\pi n_0/\lambda_0)\cdot \sin(\theta/2)$, and n_0 and λ_0 are the refractive index of the solvent and the wavelength of light in a vacuum, respectively. The angle θ is defined in Figure 1. For the special case of monodisperse Gaussian coils, the angular dependence of the particle scattering factor is such that the correct radius of gyration can be obtained at $|\mathbf{q}|\langle r_g^2\rangle^{1/2}$ considerably greater than one.

In flowing solutions, the polymer chain will deviate from its equilibrium conformation if the strength of the flow overcomes the rotational diffusion of the molecule in solution. This rotational diffusion occurs on a time scale that can be described by the characteristic relaxation time λ of the solution and is given by the following equation:

$$\lambda = \frac{[\eta]_0 \eta_s M}{RT} \tag{1}$$

where $[\eta]_0$ is the zero shear rate intrinsic viscosity of the solution, η_s is the solvent viscosity, M is the molecular weight of the polymer, R is the universal gas constant, and T is the temperature. The characteristic relaxation time given in eq 1 has been used throughout to nondimensionalize the strain rate and is related to the longest Zimm relaxation time by $\lambda = 0.422\lambda_Z$.[35] In an extensional flow, the rate of strain $\dot\epsilon$ must overcome the diffusional time constant before significant deformation will occur. Once this critical strain rate is met, at the coil−stretch transition, the chains become highly extended.[36−38] In any real extensional flow device, this transition may be smoothed considerably by finite transit times in the device and sample polydispersity.[11]

Under these flowing conditions, the deformed polymer conformation can be described by the alignment of the chains with respect to the flow direction and the degree of deformation from equilibrium dimensions. The align-

ment is described by the orientation angle χ and is defined as shown in Figure 1 for a sample extensional flow, where $\chi = 90°$ indicates complete alignment with the flow direction. The deformation is measured relative to the equilibrium dimensions. The major, minor, and neutral axis extension ratios are defined in the following way:

$$e_i = \sqrt{\frac{\langle r_i^2 \rangle_{\dot{\epsilon}\lambda}}{\langle r_i^2 \rangle_0}}, \quad i = a, b, c \tag{2}$$

where e_i is the major, minor, or neutral axis extension ratio (with $i = a$, b, or c, respectively), $\langle r_i^2 \rangle^{1/2}$ is the major, minor, or neutral axis dimension, subscript $\dot{\epsilon}\lambda$ refers to the solution undergoing extensional flow, and subscript 0 refers to the quiescent solution. The overall expansion ratio e of the polymer molecule can also be determined from the extension ratios by the following equation:

$$e = \sqrt{\frac{\langle r_g^2 \rangle_{\dot{\epsilon}\lambda}}{\langle r_g^2 \rangle_0}} = \sqrt{\frac{e_a^2 + e_b^2 + e_c^2}{3}} \tag{3}$$

where $\langle r_g^2 \rangle^{1/2}$ is the radius of gyration.

Because of the destructive interference that occurs from light scattered from different parts of the same polymer chain, the intensity of the scattered light is inversely related to the size of the chain projected onto the detector. Therefore, by changing the flow plane angle ϕ' (see Figure 1) with respect to the detector at a fixed detection angle θ, one can determine the orientation angle by examining the intensity as a function of the flow plane angle ϕ'. A maximum in the intensity ratio curve corresponds to a minimum in the projected dimension of the deformed molecule. The locations of the extrema of the intensity ratio curve yield the positions of the major and minor axes of the polymer chain with respect to the flow plane angle. A Zimm-plot-type analysis is employed for the quantitative determination of the extended chain dimensions.

Multicomponent Light Scattering. In some of the extensional flow light scattering experiments, a mixed solvent system has been used to examine the effects of solvent quality on polymer chain dynamics. These systems cannot in general be analyzed in the same way as single solvent systems. The theory for light scattering from multicomponent systems in the absence of angular dissymmetry was derived separately by Stockmayer[39] and Kirkwood and Goldberg[40] from fluctuation theory. Later, Yamakawa[41,42] extended the theory of multicomponent light scattering to account for angular dissymmetry using distribution-function theory. Following Yamakawa's construction, as shown in detail in a previous publication, the data for the multicomponent system used in this study can be described by the following set of equations:[43]

$$\lim_{c_2 \to 0} \frac{K' c_2}{\Delta R_\theta} = \frac{1}{M_{2,\mathrm{ap}}} \left[1 + \frac{16\pi^2 n^2}{3\lambda_0^2} \langle r_g^2 \rangle_{\mathrm{ap}} \sin^2(\theta/2) \right] \tag{4}$$

$$\langle r_g^2 \rangle_{\mathrm{ap}} = \frac{\langle r_g^2 \rangle}{1 - \dfrac{2M_1^2 A_{2,11}^{(1)}(c_1) c_1^2}{M_2[1 - 4M_1 A_{2,12}(c_1, c_2) c_1]}} \tag{5}$$

$$M_{2,\mathrm{ap}} = M_2(1 - 4M_1 A_{2,12} c_1 - 2M_1^2 M_2^{-1} A_{2,11}^{(1)}(c_1) c_1^2) \tag{6}$$

Subscript 1 refers to the second solvent (low molecular weight polystyrene (LMPS) in our system), subscript 2 refers to the high molecular weight polymer species (HMPS), c_i is the concentration of the species i, M_i is the molecular weight of species i, ΔR_θ is the excess Rayleigh ratio, n is the refractive index of the solution, λ_0 is the wavelength of the incident laser light, θ is the scattering angle, $A_{2,11}^{(1)}$ and $A_{2,12}$ are the second virial coefficients for species 1 and the cross coefficient between 1 and 2, respectively, and K' is the optical constant defined by the following equation:

$$K' = \frac{2\pi^2 n^2}{N_A \lambda_0^4} \left(\frac{\mathrm{d}n}{\mathrm{d}c_2} \right)^2 \tag{7}$$

where N_A is Avogadro's number. $\langle r_g^2 \rangle_{\mathrm{ap}}$ and $M_{2,\mathrm{ap}}$ are the apparent radius of gyration and the apparent molecular weight of the HMPS that are measured when the scattering data are analyzed in the usual way for single solvent systems. For the flow light scattering analysis, since we are interested only in the relative extension and expansion ratios, the apparent values are sufficient.

Dynamic Light Scattering. While the Rayleigh–Debye theory employed in the above static light scattering experiments describes the information obtained from the time-averaged intensity scattered from the polymer solution, dynamic light scattering techniques can be used to examine the time dependence of the intensity fluctuations in the scattered light. Conventionally, this technique is used to measure the diffusion of particles or molecules in quiescent suspensions and solutions. However, when applied to flowing solutions, the technique can be used to examine velocities or velocity gradients. As shown by Fuller et al.[13] and Wang et al.,[14] the homodyne scattering from particles in a liquid can be related to the movement of the particles during flow. We briefly summarize their analysis below.

Fluctuations in the intensity of the scattered light are due to concentration or density fluctuations; as time increases, these fluctuations become uncorrelated. The decay time of the autocorrelation of the intensity is then related to a characteristic time for the movement of scatterers in the fluid sample. In a quiescent fluid, this characteristic time corresponds to the diffusional time constant. The size of the molecules or particles in quiescent solution or suspension can be determined by relating the measured diffusion coefficient of the scatterers to their hydrodynamic radii through the Stokes–Einstein equation. In flow dynamic light scattering, the time constant for the decay of the autocorrelation function is related to either the velocity or the velocity gradient. In addition, the technique can also provide information about the flow type or the strength of the flow.

For a Gaussian intensity profile of the incident beam and a linear flow field of the form $\mathbf{u} = \boldsymbol{\gamma} \cdot \mathbf{X}$, where $\mathbf{u}$ is the local fluid velocity and $\mathbf{X}$ is the position, with

$$\boldsymbol{\gamma} = \begin{bmatrix} 0 & \gamma & 0 \\ \alpha\gamma & 0 & 0 \\ 0 & 0 & 0 \end{bmatrix} \tag{8}$$

where $0 < \alpha < 1$ is the flow strength parameter and γ is the magnitude of the velocity gradient, the homodyne

correlation function $F_2(\mathbf{q},t)$ is given by the following equation:[13,14]

$$F_2(\mathbf{q},t) = \beta \exp\left\{-\frac{1}{2}q^2\gamma^2L^2t^2\cos^2\frac{\theta}{2}\left[\left(\frac{1+\alpha}{2}\right)^2\sin^2 2\psi + (\cos^2\psi - \alpha\sin^2\psi)^2\right]\right\} \quad (9)$$

where β is an experimental constant that depends on the detector optics and alignment, $\mathbf{q}$ is the scattering vector, t is time, L is the characteristic beam width, and ψ is the angle between the scattering vector and the flow direction. If $\psi = 0°$, eq 9 reduces to the following:

$$F_2(\mathbf{q},t) = \beta \exp\left\{-\frac{1}{2}q^2\gamma^2L^2t^2\cos^2\frac{\theta}{2}\right\} = \beta \exp\{-[\Gamma(0°)]^2t^2\} \quad (10)$$

When $\psi = 90°$, we obtain

$$F_2(\mathbf{q},t) = \beta \exp\left\{-\frac{1}{2}q^2\gamma^2L^2t^2\alpha^2\cos^2\frac{\theta}{2}\right\} = \beta \exp\{-[\Gamma(90°)]^2t^2\} \quad (11)$$

The decay constant $\Gamma(0°)$ in eq 10 is proportional to $\mathbf{q}\gamma L$, while in eq 11, $\Gamma(90°) \sim \mathbf{q}\gamma\alpha L$. Thus, it can be seen that two measurements of the homodyne correlation function—one at $\psi = 0°$ and one at $\psi = 90°$—will yield values of the velocity gradient γ and the flow strength parameter α. For absolute determination of the velocity gradient, however, the characteristic beam width L must be known. In the present work, we have used this flow dynamic light scattering technique to provide information about the strength of the Newtonian flow, i.e., to ascertain the conditions under which end effects and three-dimensionality become important in the Newtonian flow field in the four-roll mill.

Experimental Section

Materials. The fluids examined in the flow light scattering study were solutions of nominally monodisperse high molecular weight polystyrenes of the following molecular weights (in g/mol): 3.0×10^6, 4.0×10^6, and 2.0×10^7 from Pressure Chemical and a 6.5×10^6 g/mol sample from Polymer Laboratories. All high molecular weight polystyrenes had polydispersity indices of $M_w/M_n \leq 1.30$. The HMPS samples were dissolved in either the viscous solvent dioctyl phthalate (DOP, obtained from Aldrich) or a mixed solvent consisting of a low molecular weight polystyrene (LMPS, $M_w = 5780$ g/mol, from Pressure Chemical) and DOP, denoted as LMPS/DOP. The LMPS sample had a polydispersity index of $M_w/M_n \leq 1.05$. The mixed solvent was prepared to a concentration of 13 wt % LMPS with 87 wt % DOP. This is the same solvent studied in a previous publication,[43] as well as by Solomon and Muller.[44] Solomon and Muller reported intrinsic viscometry and quiescent static and dynamic light scattering results for solutions of HMPS in this solvent which showed that it behaves as a poor solvent for polystyrene. Additionally, observations of shear-induced scattering enhancement by Lee et al. confirm its poor solvent quality.[43] The intrinsic viscosities $[\eta]_0$ for the different polymer−solvent systems have been previously determined and are well described by the following Mark−Houwink expressions: $[\eta]_0 = 0.0030M^{0.39}$ dL/g for HMPS/DOP at 13 °C, $[\eta]_0 = 0.000425M^{0.54}$ dL/g for HMPS/DOP at 25 °C, and $[\eta]_0 = 0.0070M^{0.35}$ dL/g for HMPS/LMPS/DOP at 22 °C.[29,43,44] The refractive indices of DOP and the mixed solvent are $n_{D,DOP} = 1.486$ and $n_{D,LMPS/DOP} = 1.498$, respectively.

Fluid Preparation. The samples for the light scattering experiments were carefully prepared to ensure dust-free solutions. The high molecular weight polystyrenes were first dissolved in spectrophotometric grade toluene (Aldrich) which had been filtered through 0.2 μm PTFE syringe filters (Gelman Sciences). The resulting solutions were refiltered through 1.0 μm PTFE syringe filters (Whatman) into amber bottles which were specially cleaned by acetone reflux for 40 min. The toluene was then volatilized in a vacuum oven at $T = 40$ °C to obtain clean, dry polymer. The mixed solvent was prepared in a similar manner by dissolving the LMPS in spectrophotometric grade toluene which had been filtered through 0.2 μm syringe filters and volatilized in a vacuum oven. The DOP was then added to the clean, dry HMPS and LMPS samples through 0.2 μm syringe filters. Both the mixed solvent and the single solvent solutions were allowed to dissolve in an oven at $T = 60$ °C. Once the mixed solvent was homogeneous, it was added without further preparation to the clean, dry HMPS and was allowed to mix in an oven at $T = 60$ °C. Concentrations of the solutions used for static light scattering experiments (both in quiescent and flowing solutions) were in the range $0.009c^* \leq c \leq 0.07c^*$, where $c^* = 1/[\eta]_0$.

Flow dynamic light scattering experiments were performed in a Newtonian fluid consisting of glycerin (Aldrich) and polystyrene latex spheres of nominal diameter 0.091 μm, obtained from Duke Scientific. The glycerin was hot filtered through 0.2 μm polysulfone syringe filters (Gelman Sciences) prior to addition of the spheres. The concentration of the suspension used for the dynamic light scattering experiments was 81 ppm.

Flow visualization experiments were performed in a Newtonian fluid of glycerin, seeded with polystyrene DVB (polystyrene cross-linked with 4−8% divinylbenzene) microspheres of 100−500 μm diameter from Duke Scientific. No additional preparation of either component was necessary before experimentation.

Flow Visualization. Flow visualization experiments in the four-roll mill were performed on the apparatus shown in Figure 2. The flow cell was immersed in the fluid sample contained in a glass vat. The vat was set on top of a clear Plexiglas plate so that the flow could be imaged with mirrors from below. A plane perpendicular to the axes of the rollers was illuminated by a sheet of laser light from an argon ion laser. A CCD camera was aligned for image capture perpendicular to the plane of flow and calibrated such that measurements on the captured image could be directly correlated to real dimensions. Images were captured by a frame grabber installed in a Macintosh Quadra 840AV at 30 frames/s and also directly to videotape. The images were subsequently analyzed with the software NIH Image. Seed particles were tracked during movies that were approximately 30 s in length. Streakline images such as the one shown in Figure 4 were generated from a stack of frames by taking the pixel of the minimum illumination for each position in the frames for the entire set of images. In addition to verification of the planar extensional flow, these experiments also allowed full characterization of the flow field, dimensions, and the geometry.

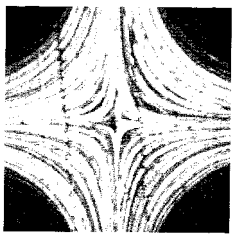

Figure 4. Streakline image of the stagnation point flow in the four-roll mill. The dark regions are the rollers of the flow device.

Light Scattering. The quiescent solution static light scattering experiments were performed in a Brookhaven Instruments system. The detection angle θ was varied by moving a photomultiplier tube mounted on a stepper-motor-controlled goniometer arm. The angular range accessible in the experiments was $20° < \theta < 150°$, giving scattering vectors in the range 6.6×10^{-3} nm$^{-1} < |\mathbf{q}| < 3.7 \times 10^{-2}$ nm^{-1}. For the higher molecular weight polymers, the angular range of 20°

$< \theta < 90°$ was used. For lower molecular weight samples, the range was $40° < \theta < 140°$. The incident laser light was provided by an Innova 70-2 argon ion laser with a wavelength of $\lambda_0 = 488$ nm. For both the quiescent and flow light scattering experiments, the scattering volume is characterized by the beam waist, calculated to be 17 μm for our optical system, and increases as the angle θ decreases from 90° (where its longest axis is approximately 34 μm) as $1/\sin\theta$ (as confirmed by an $I \sin\theta$ plot). Polymer solution samples were held in Pyrex tubes with a nominal diameter of 13 mm. The tubes were immersed in decahydronaphthalene (decalin, from Aldrich) in the light scattering vat for refractive index matching and temperature control purposes. The temperature of the samples was kept within ±0.1 °C by a recirculating water bath. The refractive index increment of the HMPS/LMPS/DOP solutions was measured by Solomon and Muller[44] to be $dn/dc_2 = 0.0980$ mL/g. For the HMPS/DOP system, the refractive index increment was determined to be $dn/dc = 0.1095$ mL/g at 488 nm from an interpolation of measurements on a Brice-Phoenix differential refractometer equipped with a mercury arc lamp (model BP-2000-V).

Flow Light Scattering. The flow light scattering measurements were performed in the Brookhaven Instruments light scattering system with modifications to allow for the inclusion of a flow cell. The extensional flow was generated by a four-roll mill device. The rollers of the four-roll mill device were immersed in the fluid sample contained in the light scattering vat. The four-roll mill was suspended from above on rotation and $x-y$ translation stages to allow movement with respect to the scattering volume and detector (Figure 3a). The location of the scattering volume was meticulously aligned with respect to the stagnation point in the flow field by use of an alignment pin, adjustable mounts, and the rotation and translation stages. The rollers were constructed of Corning 7740 glass of 20 mm diameter and attached to aluminum and stainless steel shafts. The main roller shaft was constructed of stainless steel and driven by a stepper motor. The remaining rollers were driven off the main roller by gears. The glass rollers, with $n_{D,glass} = 1.475$, were carefully refractive index matched to the solutions to eliminate undesirable reflection and refraction of the primary and scattered beams. The separation of the rollers in the flow cell was such that the centers of the rollers traced out a square 26.42 mm on a side (see Figure 3b); the circular vat containing the fluid sample had an inner diameter of 80 mm. The kinematics of the specific geometry of the four-roll mill has been the subject of an in-depth study by Higdon, who showed the effects of roller radius, roller spacing, and container size on the flow field by numerical computations.[45] The geometry we adopted is close to that of Fuller and coworkers,[11,13,46] which, although not the optimal design, was shown by Higdon to be a reasonable estimation of extensional flow within the region of interest for the light scattering studies, namely the scattering volume. The approximate extension rate $\dot{\epsilon}$ in the region between the rollers is given by

$$\dot{\epsilon} = \frac{R_0\omega}{d} \tag{12}$$

where R_0 is the radius of the rollers, ω is the angular velocity of the rollers, and d is the radius of a circle whose circumference just touches the four rollers (see Figure 3b). [47]

The flow dynamic light scattering (FDLS) experiments were performed in two flow geometries: the four-roll mill and near a single cylinder rotating about its axis. The single rotating cylinder was a solid glass rod with diameter 30 mm attached to a motor via a stainless steel shaft at the top. For both single roller and extensional flow experiments, the fluid sample was contained directly in the light scattering vat itself, and the flow device was immersed into the fluid from above. The correlations for the dynamic light scattering experiments were performed with the BI8000AT correlator card from Brookhaven Instruments.

The conformation of the polymer molecules was measured by use of time-averaged flow light scattering (FLS) techniques. The behavior of the chains was described by studying both the orientation and deformation of the polymer molecules during extensional flow. For a purely extensional flow, the orientation angle is expected to be $\chi = 90°$, indicating complete alignment of the molecules with the stretch direction. The orientation of the chains can be determined by examining the intensity of the scattered light at a fixed detection angle θ, but as a function of the flow plane angle ϕ'. The variation of ϕ' was achieved by rotation of the flow cell device on the rotation stage. For the deformation or stretching of the polymer chains, a Zimm-plot-type analysis was performed. Scattered intensity data are taken as a function of both detection angle and concentration of HMPS while keeping either the major or minor axis of the stretched chain projected onto the scattering vector for each θ. The data for the solution under flow are compared to the quiescent solution data to determine the relative amount of deformation in the two axis dimensions. More detailed descriptions of the same experimental procedure used in a steady shearing flow can be found in a previous publication.[1]

Results

Flow Visualization. The flow visualization experiments were completed to verify that a good approximation of a planar extensional flow field was being generated near the stagnation point of the four-roll mill flow cell. Figure 4 shows an image of the streaklines generated by the flow device. The shape of the lines agrees well with the expected shape with slight deviations near the roller walls. Because of slight imperfections in the concentricity of the rollers, there are slight variations in the location of the stagnation point in the extensional flow field with time. The variation in roller diameter or eccentricity along a single roller was less than 4 μm, and the movement of the stagnation point near the center of the rollers is expected to be less than 8 μm. The movement of the stagnation point was measured by using flow visualization, and the stagnation point was determined to remain within the scattering volume for the light scattering experiments.

Flow Dynamic Light Scattering. In addition to the flow visualization experiments, flow dynamic light scattering experiments were performed in order to further confirm the extensional flow field and to determine when end effects and three-dimensionality become important in the four-roll mill for a Newtonian fluid. The technique was first tested by examining a seeded Newtonian fluid (81 ppm polystyrene latex spheres in glycerin) with flow near a single rotating cylinder in an "infinite" medium. Because the flow field is known in this geometry, the efficacy for this method of determining the velocity gradient or shear rate could be checked. As seen in Figure 5, a plot of the decay constant Γ versus $1/r^2$, where r is the radial position away from the center of the rotating cylinder, gives a straight line for each angular velocity investigated. The data are well fit by straight lines. There is slight deviation, however, from the fits at small values of $1/r^2$ (or large values of r) due to wall effects (i.e., the light scattering vat). The decay constant Γ is related to the velocity gradient according to eq 10. For a single rotating roller, the velocity gradient is given by

$$\gamma = -\frac{2\omega R^2}{r^2} \tag{13}$$

where R is the roller radius. The slope of the straight lines in Figure 5 is then proportional to the angular velocity ω. A comparison of the ratios of the angular

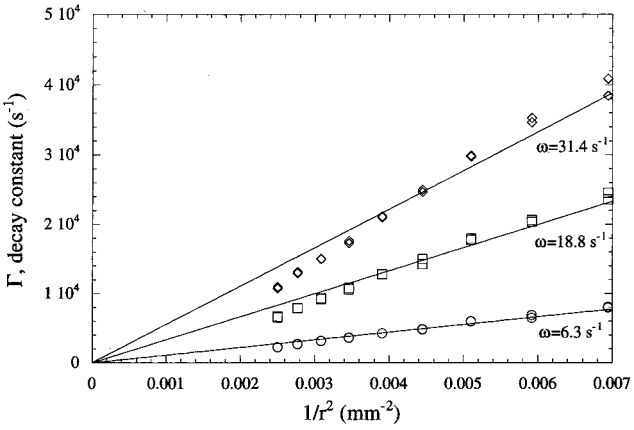

Figure 5. Decay constant Γ versus $1/r^2$ for single rotating cylinder in Newtonian fluid for various angular velocities. r is the distance away from the center of the cylinder.

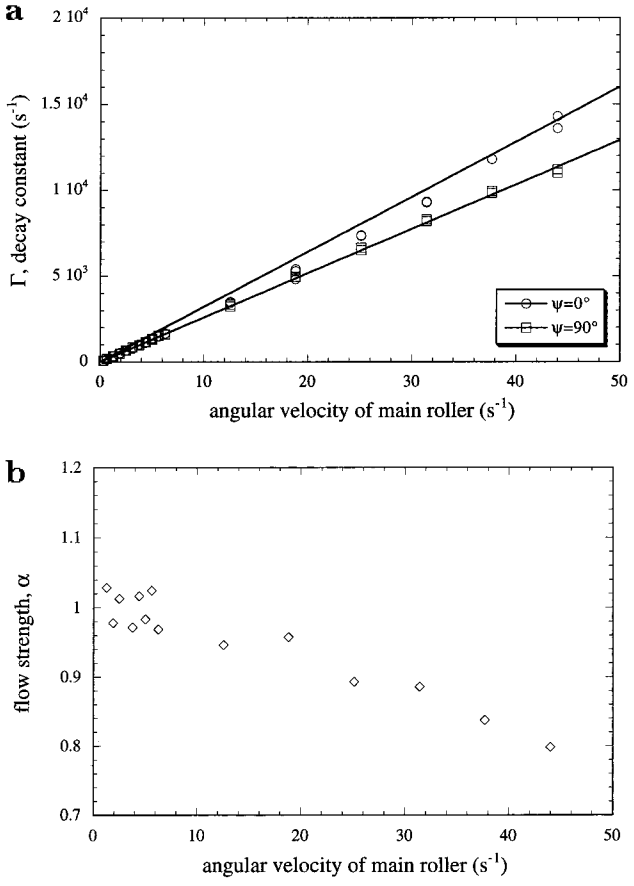

Figure 6. (a) Decay constant Γ versus angular velocity of main roller in extensional flow (Newtonian fluid) for $\psi = 0°$ and $\psi = 90°$. (b) Flow strength parameter α versus angular velocity of main roller in extensional flow.

velocities to those of the slopes shows that this relationship holds to within 0.5%.

The extensional FDLS experiments were performed in the four-roll mill flow device for both $\psi = 0°$ and $\psi = 90°$ (see Figure 6a). For $\psi = 0°$, $\Gamma = q\gamma L$ while for $\psi = 90°$, $\Gamma = q\gamma\alpha L$. The data are well fit by straight lines. In addition to the velocity gradient, a measurement of the strength of the flow field could be extracted from the FDLS experiments. For a pure extensional flow, the flow strength parameter has a value of $\alpha = 1$; a purely shearing flow has $\alpha = 0$. Figure 6b shows the flow

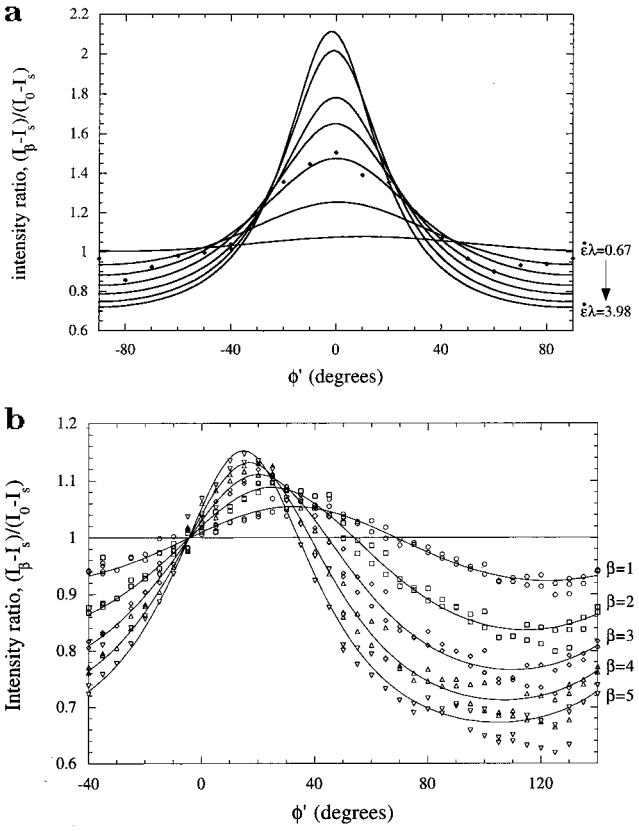

Figure 7. Intensity ratio plots: (a) intensity ratio versus ϕ' for various strain rates for 2×10^7 g/mol HMPS/DOP at $T = 25$ °C, $\theta = 80°$ in extensional flow; for clarity, only fits to the data are shown for all but one strain rate ($\dot{\epsilon}\lambda = 1.33$). (b) Intensity ratio versus ϕ' for various shear rates for 3×10^6 g/mol HMPS/DOP at $T = 25$ °C, $\theta = 80°$ in shear flow.

strength parameter, α, as a function of the rotation rate of the main roller for the extensional flow geometry determined from the data in Figure 6a. We see that at the lower rotation rates the flow is almost purely extensional, giving values of α close to unity. As the rotation rate is increased, the flow begins to deviate from $\alpha = 1$. From visual observations, this can be seen to be due to free surface effects; the free surface at the top of the vat distorts when a high roller rotation rate is applied. This gives rise to velocity components that are out of plane and that in turn induce deviations from purely extensional flow. The roller rates for the flow light scattering (FLS) experiments were therefore kept below an angular velocity of $\omega \approx 25$ s^{-1} in order to maintain a reasonably good elongational flow field.

Orientation. Since there are only straining forces acting in one direction for a pure elongational flow, the chains are expected to orient completely in the stretch direction for all strain rates. This test serves as an additional check on the flow field. The intensity ratio is measured as a function of the flow plane angle ϕ' at a fixed detection angle θ, as described in the Experimental Section. Figure 7a shows intensity ratio versus ϕ' curves taken at a detection angle of $\theta = 80°$ at various strain rates for 2×10^7 g/mol HMPS/DOP at $T = 25$ °C. As seen in the figure, the maxima of the curves for all strain rates fall at $\phi' = 0°$, giving orientation angles of $\chi = 90 \pm 2°$ (complete alignment with the stretch direction), as expected. In addition to the orientation information, this type of plot also provides qualitative information about the size and shape of the deformed

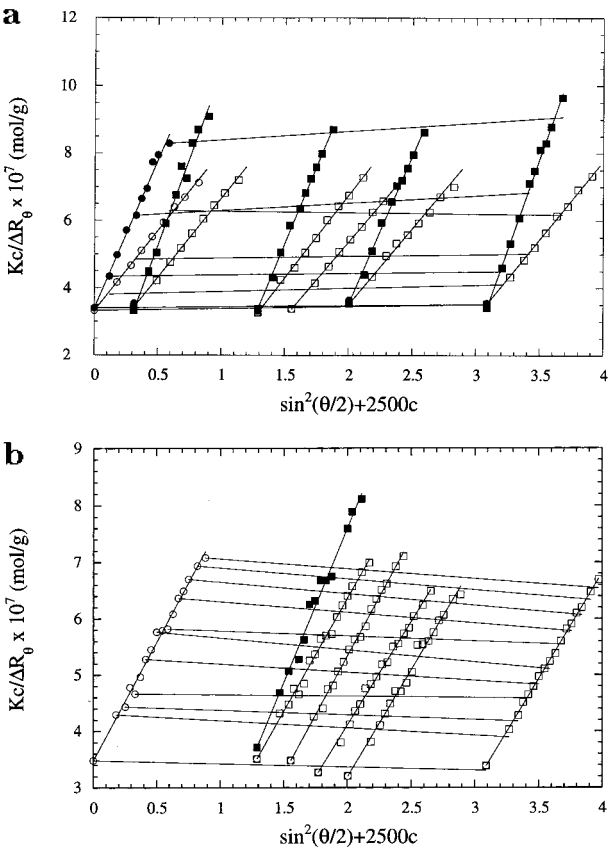

Figure 8. Zimm plot with flow data superposed: (a) shear data for 3×10^6 g/mol HMPS/DOP at $T = 25$ °C at $\beta = 3.17$ for all concentrations; (b) extensional data for 3×10^6 g/mol HMPS/DOP at $T = 13$ °C at $\dot{\epsilon}\lambda = 1.0$ for $c = 0.051c^*$.

polymer chains in flow. The amount of deviation from an intensity ratio of unity corresponds to the amount of deformation of a polymer chain from its equilibrium conformation. Figure 7b shows the same type of intensity ratio plot for a 3×10^6 g/mol HMPS/DOP sample at $T = 25$ °C undergoing a steady shearing flow. The shapes of the curves are qualitatively different. In the shearing flow, the maxima occur away from 0°, and the growth of the maxima and minima is more gradual. The sharper extrema in the extensional flow indicates the polymer chain is much more extended here.

Deformation. A quantitative measurement of the deformation of the polymer chains can be obtained by employing a Zimm-plot-type analysis. Figure 8a illustrates this analysis, showing a static light scattering plot for 3×10^6 g/mol HMPS/DOP at 25 °C in quiescent solution (open markers) with data taken in a Couette shearing cell (filled markers) at a dimensionless shear rate of $\beta = \lambda\dot{\gamma} = 3.17$ for the major axis of the deformed polymer molecule overlaid. At each of the concentrations, the slopes of the shear data lines are larger than those of the quiescent solution data, giving an infinite dilution extrapolation with a larger slope in shear. Since the slope of the $c = 0$ extrapolation yields a measurement of the projected dimension of the polymer chain, a ratio of the flow to quiescent solution slopes provides the major axis extension ratio. In shear flow, Link and Springer[29] and Lee et al.[1] show that, for concentrations below $0.1c^*$, concentration effects are negligible so that extrapolations to zero concentration are unnecessary as long as $c < 0.1c^*$. The Zimm-plot-type construction can also be performed for a solution in extensional flow in order to extract the extension ratios as a function of strain rate. While in extensional flows at high strain rates Carrington et al. and Dunlap and Leal demonstrate that the concentration required to observe truly dilute behavior may be as low as $0.01c^*$,[22,25] at the relatively modest dimensionless strain rates we achieve, we expect dilute behavior for our solutions for which $0.009c^* \leq c \leq 0.07c^*$. Figure 8b shows a quiescent solution Zimm plot with extensional data at $\dot{\epsilon}\lambda = 1.0$ superposed for a single concentration of $0.051c^*$ in 3×10^6 g/mol HMPS in DOP at $T = 13$ °C. The data for the major axis extension ratios versus $\dot{\epsilon}\lambda$ obtained by the Zimm plot method are shown in Figure 9 for a 2×10^7 g/mol HMPS/DOP solution at 25 °C. Also included in the plot are the results for the same solution in shear flow. The stronger extensional flow is able to deform the polymer chains more than does the shear flow. Elastic dumbbell model predictions are included in the plot for comparison. Although the polymer chains are experiencing more deformation in the stronger elongational flow than in the steady shear case, the extended dimensions are still greatly overpredicted by the elastic dumbbell model.

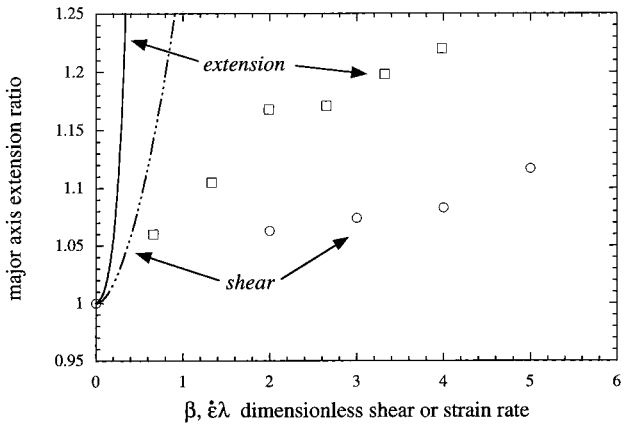

Figure 9. Major axis extension ratio for 2×10^7 g/mol HMPS/DOP at $T = 25$ °C versus β or $\dot{\epsilon}\lambda$ comparing shear and extensional flows (with elastic dumbbell model predictions for each).

The effect of solvent quality on polymer chain deformation was also investigated. Because the light scattering experiments impose such strict constraints on refractive index matching between the glass rollers and the fluid samples, the choice of solvents was limited to DOP and the mixed solvent LMPS/DOP. However, the range of solvent qualities was extended by varying the temperature. The solvent qualities of the solutions were characterized both by excluded-volume exponents (determined by intrinsic viscometry) and by critical shear rates for the onset of shear-induced scattering enhancement (cf. Table 2 in Lee and Muller[43]). The excluded-volume exponent ν, defined by $\langle r_g^2 \rangle^{1/2} \sim M^\nu$, ranges from 0.51 for DOP at 25 °C to 0.45 for LMPS/DOP at 22 °C. For both solvents, the solvent quality improves with increasing temperature. Figure 10 shows the extension ratio for a 3×10^6 g/mol HMPS in this range of solvents. As the quality of the solvent increases, we see a decrease in the amount of deformation measured for the polymer chains. This trend is in qualitative agreement with the results seen for the shearing flow in a previous publication.[43]

The effect of molecular weight on polymer chain deformation in extensional flow was also examined. A range of molecular weights of almost a decade was

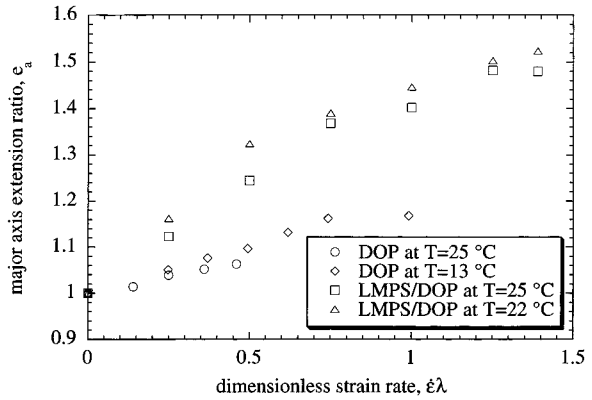

Figure 10. Solvent quality effects on deformation in extensional flow for 3×10^6 g/mol HMPS in various solvent systems.

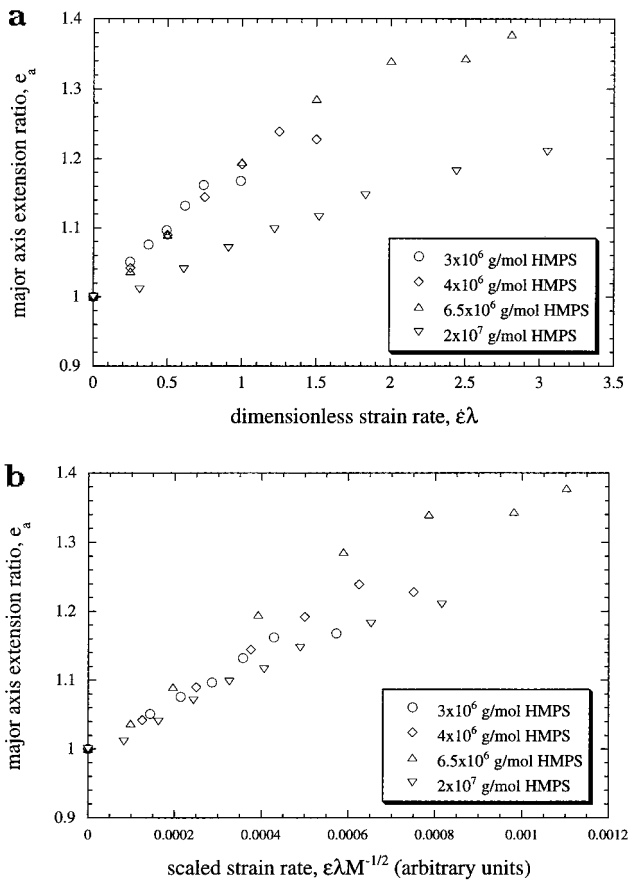

Figure 11. Molecular weight effects of HMPS/DOP at T = 13 °C in extensional flow: (a) e_a versus $\dot{\epsilon}\lambda$, (b) e_a versus $\dot{\epsilon}\lambda M^{-1/2}$.

examined in DOP at 13 °C, where the solvent behaves as a poor solvent. This low temperature was required to achieve a reasonable dimensionless strain rate range while maintaining a good extensional flow for the lower molecular weight samples. As seen in Figure 11a, the deformation of the polymer chains decreases as the molecular weight is increased when plotted with the dimensionless strain rate $\dot{\epsilon}\lambda$. We can rescale the dimensionless strain rate with the molecular weight M to collapse all the extensional data to a master curve if we plot the major axis extension ratio as a function of $\dot{\epsilon}\lambda M^{-1/2}$ rather than $\dot{\epsilon}\lambda$, as shown in Figure 11b. We note that the failure of the elastic dumbbell model to capture the molecular weight scaling was also observed in shearing flow in an earlier study.[1]

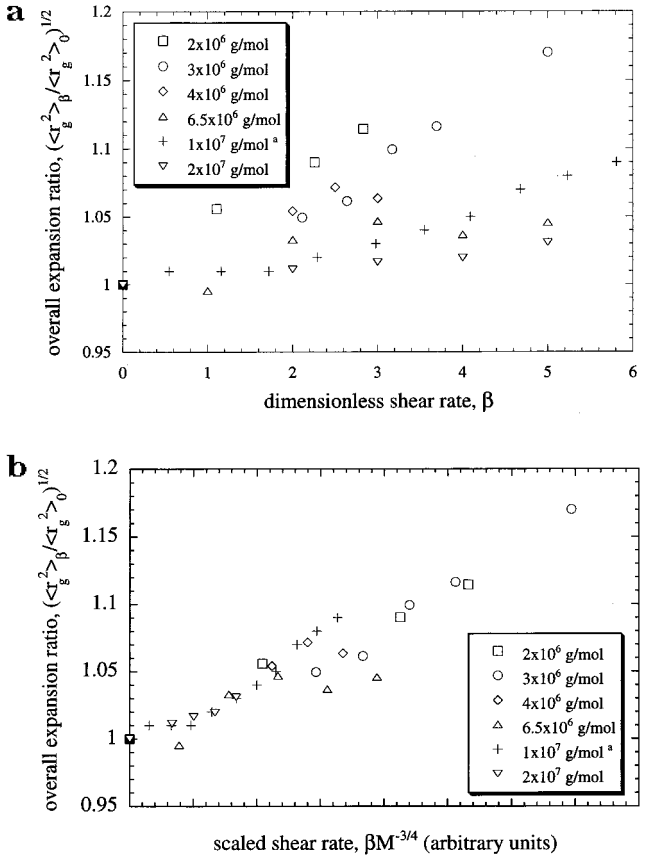

Figure 12. Molecular weight effects of HMPS/DOP at T = 25 °C in shear flow: (a) e versus β, (b) e versus $\beta M^{-3/4}$. [a]Note: data identified as 1×10^7 g/mol are replotted from Link and Springer.[29]

In the shear flow case, the overall expansion ratio for HMPS in DOP at 25 °C also decreased with increasing molecular weight at a fixed dimensionless shear rate β; that data, reproduced here in Figure 12a, can be collapsed when plotted as a function of $\beta M^{-3/4}$ rather than β as shown by the master curve in Figure 12b. There are slight deviations from both master curves for some molecular weight samples. We attribute these deviations to small differences in the polydispersity index for each of the nominally monodisperse samples studied. A more detailed discussion of polydispersity effects can be found in ref 1.

Discussion

We have investigated the stretching of dilute polymer chains in the planar extensional flow generated in a four-roll mill. The onset of significant end effects and the three-dimensionality in the Newtonian flow field, as determined by flow dynamic light scattering experiments, have limited these experiments to dimensionless strain rates that are relatively modest: our highest strain rates ($\dot{\epsilon}\lambda \approx 4$) are below those at which other authors report saturation of the birefringence[22,25,48] and below where Menasveta and Hoagland report a plateau in the radius of gyration.[30] (They are also significantly below strain rates at which chain halving has been reported.[19,20]) On the basis of these earlier studies, we anticipate that we are at conditions below those at which flow modification due to chain stretching occurs. Flow light scattering measurements at higher dimensionless strain rates (achievable in a different geometry) along with simultaneous measurements of

the flow field were beyond the scope of the present study.

The flow light scattering results presented here provide a direct measure of the average orientation and deformation of high molecular weight polystyrene chains in dilute solution undergoing a steady, extensional flow. The spatial resolution of the technique is comparable to that of techniques that have been used to probe the homogeneity of the birefringence and velocity fields.[22,25] Hence, we expect our measurements to be sufficiently localized near the stagnation point that they are not dominated by molecules experiencing relatively little strain.

Under all conditions examined, the chains align completely with the stretch direction. While the extensional field examined here is able to deform the chains more than the weaker shear flow studied previously,[1] the magnitudes of the deformations measured are significantly lower than predicted by a simple elastic dumbbell model. Both solvent quality and polymer molecular weight were varied systematically and had significant effects on the extension ratio. Lower molecular weight chains and chains in poorer solvents consistently exhibited larger extension ratios at a given dimensionless strain rate $\dot{\epsilon}\lambda$. That is, the Zimm scaling did not collapse the extension ratio data (cf. Figure 11). Both of these trends are qualitatively consistent with our earlier observations of chain deformation in steady shearing flow.[1,43]

Our results are roughly consistent with the earlier flow light scattering studies of synthetic polymer solutions in extensional flows. At dimensionless strain rates that are a factor of 4 or 5 higher than those achieved here, Menasveta and Hoagland reported an extension ratio of approximately two for a polystyrene sample similar to our highest molecular weight sample.[30] Also at a much higher strain rate, Smith et al.[15] reported extension ratios of 1.5 to 4 for polydisperse polyisobutylene samples; significantly, they also reported that at comparable dimensionless strain rates the lower molecular weight sample exhibited the higher extension ratio—the same trend we report in Figure 11a.

Comparing our results to the DNA fluorescence microscopy experiments of Chu and co-workers,[31] we note that at dimensionless strain rates comparable to those achieved here, the average DNA chain extension approached half its fully extended length after roughly three units of strain. This corresponds to a significantly greater extension ratio than observed here for any of our polystyrene samples. Given the extensive broadening of the distribution of chain conformations observed in the DNA experiments, one can question whether our light scattering experiments are simply "missing" the subset of chains that are near full extension. That is, as the chains become stretched, one must make scattering measurements at correspondingly lower scattering angles to ensure the $|\mathbf{q}|\langle r_g^2\rangle^{1/2} < 1$ criterion for extrapolation of the inverse particle scattering factor is met. Instrumental limitations certainly preclude the possibility of our measuring chains of the 2.0×10^7 g/mol PS which have quadrupled or more in projected radius, but several considerations suggest that we are not "missing" chains. First, the total scattering was consistent in every case with the known concentration of scatterers, and we saw no anomalous increase in the molecular weights determined through a Zimm plot analysis on the flow data. (Menasveta and Hoagland did report such an increase in the molecular weight but attributed it to the optical anisotropy of the flow-oriented solution and used the shift to make a polarizability correction to their reported extension ratios.) Moreover, even the much smaller 3.0×10^6 g/mol PS chains show little average stretching; for these chains we do not see even our average measure of extension approaching the resolution limits of our light scattering instrument.

The above points to real differences in the behavior of polystyrene and DNA in extensional flow at low strain rates. The orders of magnitude difference in the number of persistence lengths between the two polymers, as well as our observed increase in extension ratio with decreasing molecular weight, suggests the importance of intramolecular entanglements. The greater number of self-entanglements may simply slow the stretching dynamics, and more strain units than were realized in our four-roll mill may be needed to stretch the PS. In addition, the relative ratio of polymer segment size to solvent size is also vastly different between the DNA and the PS: there may be significant differences in the polymer−solvent (and polymer−polymer) friction between the two cases. Finally, the sensitivity of extension ratio to solvent quality also indicates the need to include polymer−solvent interactions in any modeling of the dynamics.

Acknowledgment. This work was supported in part by the Director, Office of Energy Research, Office of Basic Energy Sciences, Materials Sciences Division, of the U.S. Department of Energy under contract DE-AC03-76SF00098. The authors also acknowledge gifts to support polymer research from Raychem and helpful discussions with M. J. Solomon.

References and Notes

(1) Lee, E. C.; Solomon, M. J.; Muller, S. J. *Macromolecules* **1997**, *30*, 7313−7321.
(2) Lumley, J. L. *Phys. Fluids* **1977**, *20*, s64−s71.
(3) Cottrell, F. R. *An Experimental Study of the Conformation of Polyisobutylene in a Hydrodynamic Shear Field*; Massachusetts Institute of Technology: Cambridge, 1968; p 307.
(4) Pope, D. P.; Keller, A. *Colloid Polym. Sci.* **1978**, *256*, 751−756.
(5) Farrell, C. J.; Keller, A.; Miles, M. J.; Pope, D. P. *Polymer* **1980**, *21*, 1292−1294.
(6) Miles, M. J.; Keller, A. *Polymer* **1980**, *21*, 1295−1298.
(7) Keller, A.; Odell, A. J. *Colloid Polym. Sci.* **1985**, *263*, 181−201.
(8) Taylor, G. I. *Proc. R. Soc. London* **1934**, *29*, 501−523.
(9) Bentley, B. J.; Leal, L. G. *J. Fluid Mech.* **1986**, *167*, 219−240.
(10) Feng, J.; Leal, L. G. *J. Non-Newtonian Fluid Mech.* **1997**, *72*, 187−218.
(11) Fuller, G. G.; Leal, L. G. *Rheol. Acta* **1980**, *19*, 580−600.
(12) Fuller, G. G.; Leal, L. G. *J. Non-Newtonian Fluid Mech.* **1981**, *8*, 271−310.
(13) Fuller, G. G.; Rallison, J. M.; Schmidt, R. L.; Leal, L. G. *J. Fluid Mech.* **1980**, *100*, 555−575.
(14) Wang, J. J.; Yavich, D.; Leal, L. G. *Phys. Fluids* **1994**, *6*, 3519−3534.
(15) Smith, K. A.; Merrill, E. W.; Peebles, L. H.; Banijamali, S. H. *Colloq. Int. C.N.R.S.* **1975**, *233*, 341−344.
(16) Tirtaatmadja, V.; Sridhar, T. *J. Rheol.* **1993**, *37*, 1081−1102.
(17) James, D. F.; Sridhar, T. *J. Rheol.* **1995**, *39*, 713−724.
(18) Cathey, C. A.; Fuller, G. G. *J. Non-Newtonian Fluid Mech.* **1990**, *34*, 63−88.
(19) Odell, J. A.; Keller, A. *J. Polym. Sci., Part B: Polym. Phys.* **1986**, *24*, 1889−1916.
(20) Odell, J. A.; Keller, A.; Miles, M. J. *Polym. Commun.* **1983**, *24*, 7−10.
(21) Odell, J. A.; Muller, A. J.; Narh, K. A.; Keller, A. *Macromolecules* **1990**, *23*, 3092−3103.

(22) Carrington, S. P.; Tatham, J. P.; Odell, J. A.; Saez, A. E. *Polymer* **1997**, *38*, 4151−4164.
(23) Carrington, S. P.; Tatham, J. P.; Odell, J. A.; Saez, A. E. *Polymer* **1997**, *38*, 4595−4607.
(24) Feng, J.; Leal, L. G. *J. Non-Newtonian Fluid Mech.* **1997**, *72*, 187−218.
(25) Dunlap, P. N.; Leal, L. G. *J. Non-Newtonian Fluid Mech.* **1987**, *23*, 5−48.
(26) Peterlin, A. *J. Polym. Sci.* **1957**, *23*, 189−198.
(27) Cottrell, F. R.; Merrill, E. W.; Smith, K. A. *J. Polym. Sci., Part A-2* **1969**, *7*, 1415−1434.
(28) Link, A.; Zisenis, M.; Protzl, B.; Springer, J. *Makromol. Chem., Macromol. Symp.* **1992**, *61*, 358−376.
(29) Link, A.; Springer, J. *Macromolecules* **1993**, *26*, 464−471.
(30) Menasveta, M. J.; Hoagland, D. A. *Macromolecules* **1991**, *24*, 3427−3433.
(31) Perkins, T. T.; Smith, D. E.; Chu, S. *Science* **1997**, *276*, 2016−2021.
(32) Larson, R. G.; Perkins, T. T.; Smith, D. E.; Chu, S. *Phys. Rev. E* **1997**, *55*, 1794−1797.
(33) Quake, S. R.; Babcock, H.; Chu, S. *Nature* **1997**, *388*, 151−154.
(34) Perkins, T. T.; Quake, S. R.; Smith, D. E.; Chu, S. *Science* **1994**, *264*, 822−826.
(35) Zimm, B. H. *J. Chem. Phys.* **1956**, *24*, 269−278.
(36) de Gennes, P. G. *J. Chem. Phys.* **1974**, *60*, 5030−5042.
(37) de Gennes, P. G. *Scaling Concepts in Polymer Physics*; Cornell University Press: Ithaca, NY, 1979.
(38) Larson, R. G. *Constitutive Equations for Polymer Melts and Solutions*; Butterworth Publishers: Stoneharm, MA, 1988.
(39) Stockmayer, W. H. *J. Chem. Phys.* **1950**, *18*, 58−61.
(40) Kirkwood, J. G.; Goldberg, R. J. *J. Chem. Phys.* **1950**, *18*, 54−57.
(41) Yamakawa, H. *J. Chem. Phys.* **1967**, *46*, 973−981.
(42) Yamakawa, H. *Modern Theory of Polymer Solutions*; Harper and Row: New York, 1971.
(43) Lee, E. C.; Muller, S. J. *Polymer* **1999**, *40*, 2501−2510.
(44) Solomon, M. J.; Muller, S. J. *J. Polym. Sci., Part B: Polym. Phys.* **1996**, *34*, 181−192.
(45) Higdon, J. J. L. *Phys. Fluids A* **1993**, *5*, 274−276.
(46) Fuller, G. G.; Leal, L. G. *J. Polym. Sci., Polym. Phys. Ed.* **1981**, *19*, 557−587.
(47) Pope, D. P.; Keller, A. *Colloid Polym. Sci.* **1977**, *255*, 633−643.
(48) Carrington, S. P.; Odell, J. A. *J. Non-Newtonian Fluid Mech.* **1996**, *67*, 269−283.

MA981277A